

Entorhinal cortical Island cells regulate temporal association learning with long trace period

Jun Yokose,^{1,3} William D. Marks,^{1,3} Naoki Yamamoto,¹ Sachie K. Ogawa,¹ and Takashi Kitamura^{1,2}

¹Department of Psychiatry, ²Department of Neuroscience, University of Texas Southwestern Medical Center, Dallas, Texas 75390, USA

Temporal association learning (TAL) allows for the linkage of distinct, nonsynchronous events across a period of time. This function is driven by neural interactions in the entorhinal cortical–hippocampal network, especially the neural input from the pyramidal cells in layer III of medial entorhinal cortex (MECIII) to hippocampal CA1 is crucial for TAL. Successful TAL depends on the strength of event stimuli and the duration of the temporal gap between events. Whereas it has been demonstrated that the neural input from pyramidal cells in layer II of MEC, referred to as Island cells, to inhibitory neurons in dorsal hippocampal CA1 controls TAL when the strength of event stimuli is weak, it remains unknown whether Island cells regulate TAL with long trace periods as well. To understand the role of Island cells in regulating the duration of the learnable trace period in TAL, we used Pavlovian trace fear conditioning (TFC) with a 60-sec long trace period (long trace fear conditioning [L-TFC]) coupled with optogenetic and chemogenetic neural activity manipulations as well as cell type-specific neural ablation. We found that ablation of Island cells in MECII partially increases L-TFC performance. Chemogenetic manipulation of Island cells causes differential effectiveness in Island cell activity and leads to a circuit imbalance that disrupts L-TFC. However, optogenetic terminal inhibition of Island cell input to dorsal hippocampal CA1 during the temporal association period allows for long trace intervals to be learned in TFC. These results demonstrate that Island cells have a critical role in regulating the duration of time bridgeable between associated events in TAL.

The linkage of temporally discontinuous events, called temporal association learning (TAL), is an essential function for episodic memory formation; for animals, when an event took place, and in what order a series of events occurred is directly linked to adaptation to continuous changes in the environment (Eichenbaum 2000; Tulving 2002a,b; Kitamura et al. 2015a; Kitamura 2017; Pilkiw and Takehara-Nishiuchi 2018). The entorhinal cortical–hippocampal (EC-HPC) network in particular is currently considered to bridge the temporal discontinuity between events (Solomon et al. 1986; Moyer et al. 1990; Wallenstein et al. 1998; McEchron et al. 1999; Eichenbaum 2000; Huerta et al. 2000; Ryou et al. 2001; Takehara et al. 2003; Chowdhury et al. 2005; Esclassan et al. 2009; Morrissey et al. 2012; Suter et al. 2013; Sellami et al. 2017; Wilmot et al. 2019).

Two major excitatory inputs to HPC arise from the superficial layers of the EC (Fig. 1A), forming the direct (monosynaptic), and indirect (trisynaptic) pathways (Amaral and Witter 1989; Amaral and Lavenex 2007; Kitamura 2017; Kitamura et al. 2017). While pyramidal cells in EC layer III (ECIII cells) project directly to CA1 (Kohara et al. 2014; Kitamura et al. 2015b), the trisynaptic pathway originates from excitatory Reelin⁺ stellate cells in EC layer II (ECII) projecting directly to DG, CA3, and CA2 (Fig. 1B; Tamamaki and Nojyo 1993; Varga et al. 2010). CalbindinD-28K⁺/Wolfram syndrome 1 (Wfs1)⁺ pyramidal cells, another excitatory neural population in EC layer II called “Island cells,” form cell clusters along the ECII/ECI border (Alonso and Klink 1993; Fujimaru and Kosaka 1996; Klink and Alonso 1997; Kawano et al. 2009; Varga et al. 2010; Kitamura et al. 2014; Ray et al. 2014) and directly project to the GABAergic interneurons of stratum lacunosum (SL-INs) in

HPC CA1 and drive feedforward inhibition to HPC CA1 pyramidal cells (Fig. 1B; Kitamura et al. 2014; Surmeli et al. 2016; Kitamura 2017; Ohara et al. 2018; Yang et al. 2018; Zutshi et al. 2018).

Trace fear conditioning (TFC) has been established as one suitable animal model for TAL (Fendt and Fanselow 1999; Maren 2001; Kim and Jung 2006) that can be also used as a translational bridge between animal and human learning (Clark and Squire 1998; Buchel and Dolan 2000; Delgado et al. 2006). Lesion, pharmacological, molecular, and optogenetic manipulation, as well as disease models in medial entorhinal cortex (MEC), demonstrate that MEC is crucial for TFC and temporal learning (Ryou et al. 2001; Woodruff-Pak 2001; Runyan et al. 2004; Esclassan et al. 2009; Gilmartin and Helmstetter 2010; Suh et al. 2011; Morrissey et al. 2012; Shu et al. 2016; Hales et al. 2018; Yang et al. 2018; Heys et al. 2020). Specifically, MECIII inputs into the HPC CA1 pyramidal cells are essential for the formation of TFC (Yoshida et al. 2008; Suh et al. 2011; Kitamura et al. 2014; Kitamura 2017). However, the temporal association function driven by MECIII neurons must be regulated for optimal adaptive memory formation, as too strong an association of a particular pair of events may interfere with associations of other useful pairs, whereas too weak an association for a given pair of events, in terms of weaker impact of events or longer duration of temporal gap between events, would not result in an effective memory (Kitamura et al. 2015a; Marks et al. 2020). In a naturalistic context, this would mean that more distant/quieter sounds, less intense somatic sensations (e.g., pain),

³These authors contributed equally to this work.

Corresponding author: takashi.kitamura@utsouthwestern.edu

Article is online at <http://www.learnmem.org/cgi/doi/10.1101/lm.052589.120>.

© 2021 Yokose et al. This article is distributed exclusively by Cold Spring Harbor Laboratory Press for the first 12 months after the full-issue publication date (see <http://learnmem.cshlp.org/site/misc/terms.xhtml>). After 12 months, it is available under a Creative Commons License (Attribution-NonCommercial 4.0 International), as described at <http://creativecommons.org/licenses/by-nc/4.0/>.

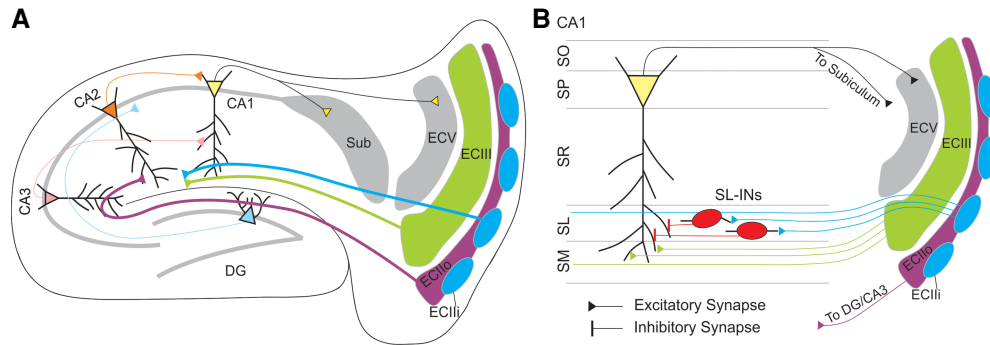


Figure 1. Circuit schematic diagram of the medial entorhinal cortex (MEC)–hippocampal (HPC) circuit. (A) Major projections in the entorhinal cortical (EC)–HPC network. ECIII neurons (green) project directly to CA1. ECII Ocean cells (ECIIo, purple) project to the dentate gyrus (DG) (light blue)/CA3 (pink) initiating the trisynaptic pathway. ECII Island cells (ECIIi, blue) project directly into CA1. (B) ECIII projections (green) excite the distal portions of CA1 pyramidal cells in stratum moleculare (SM). Island cells (ECIIi, blue) excite the interneurons of stratum lacunosum (SL-INs, red), which in turn inhibit the distal dendrites of CA1 pyramidal cells in SL.

or increased temporal distance between any two events would signal that the events are less likely to be causally associated, therefore less relevant, and less likely to be stored and recalled. In fact, successful TFC depends on the strength of event stimuli and duration of temporal gap between events (Stiedl and Spiess 1997; Misane et al. 2005; Kitamura et al. 2014; Kitamura 2017). However, the underlying regulatory mechanism for TAL remains hidden. Previously we demonstrated that feedforward inhibition by Island cells acts as a gating controller for the MECIII inputs to the distal dendrites of HPC CA1 pyramidal cells in stratum moleculare (SM) (Kitamura et al. 2014) to control TFC when weaker (in this case diminished footshock intensity) unconditioned stimuli were delivered for TFC, indicating that Island cell activity controls the temporal association when the strength of two discontinuous events are relatively weaker. However, the way in which the EC–HPC network regulates TFC with a longer trace period still remains unknown. Because the activation of Island cells would result in a net inhibitory effect on the local network in CA1, imposing a tight and specific regulation on associations of events across the temporal gap in TAL (Crestani et al. 2002; Moore et al. 2010; Kitamura et al. 2014, 2015b), we hypothesized that the length of the temporal gap between events would also be modulated by this mechanism. In this study, we examined the role of the regulatory input to this circuit arising specifically from the Island cells in the MECII using apoptotic elimination of Island cells, chemogenetic neural inhibition, and optogenetic terminal inhibition methods within an L-TFC protocol to give a thorough and complete assessment of the circuit involvement while considering each technique’s unique features.

Results

Trace fear conditioning with long CS–US contingencies in mice

In the conditioning session of TFC on day 1, we subjected two groups of C57BL/6j mice to two different TFC protocols in which after a 240-sec acclimation, a 20-sec conditioned stimulus ([CS]; tone, 5 kHz, 80 dB) is followed by a 2-sec footshock as the unconditioned stimulus ([US]; shock, 1.0 mA, 2 sec) three times with either 20 sec as a naturally associative TFC or 60-sec trace periods separating the CS and US as a long TFC (L-TFC) that is harder to associate (Fig. 2A,B). Both groups exhibited the freezing response within the conditioning protocols (Fig. 2A,B, base [averaged freezing% during the acclimation]) versus following each time point (20-sec group: one-way analysis of variance [ANOVA], $F_{(23,264)} =$

14.44, $P < 0.0001$; 60-sec group: one-way ANOVA, $F_{(29,360)} = 15.68$, $P < 0.0001$). In the testing session of TFC on day 2, we subjected the mice to a paradigm in which, following a 240-sec acclimation as a baseline, a 60-sec CS was presented three times with 180-sec intertone intervals in a different context (Fig. 2C). While both groups showed significant enhancement of the freezing responses during the tone period compared with those in the baseline period (paired t -test, base vs. tone in 20-sec group, $t_{11} = 7.39$, $P < 0.0001$; base vs. tone in 60-sec group, $t_{12} = 3.62$, $P < 0.004$), mice conditioned with the 60-sec L-TFC protocol showed significantly lower freezing responses during both the tone period (unpaired t -test, $t_{23} = 3.44$, $P < 0.002$) and the first minute post-tone period (unpaired t -test, $t_{23} = 2.66$, $P < 0.01$) (Fig. 2D) compared with the performance of the mice conditioned with the 20-sec

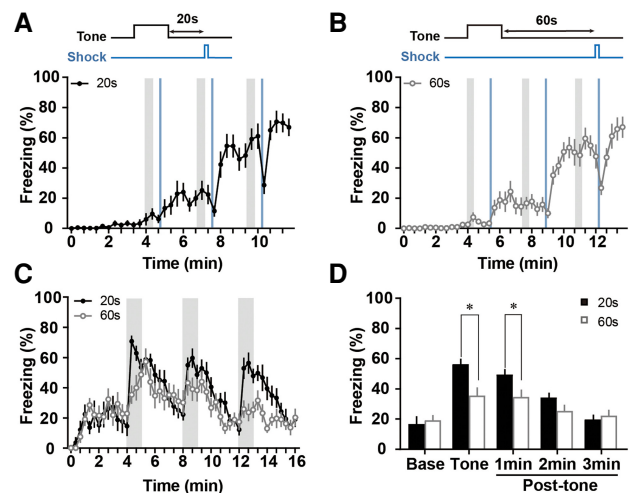


Figure 2. Trace fear conditioning (TFC) with 20- and 60-sec trace periods in mice. (A,B) Time course of freezing responses in wild-type (WT) mice during the conditioning session with a 20-sec trace period ($n = 2$) (A) and with a 60-sec trace period ($n = 13$) (B) on day 1. Gray and blue bars represent tone and shock, respectively. (C) Time course of freezing responses in both 20- and 60-sec trace groups during the testing session on day 2. Gray bars indicate 60-sec tone representations. (D) The averaged freezing responses over the three bins during each tone period and that of the first 1-min, second and third post-tone periods. Means \pm SEM. One-way analysis of variance (ANOVA) for A and B. Two-way repeated measure (RM) ANOVA for C. (*) $P < 0.05$ by unpaired t -test for D.

TFC protocol. This indicates that the longer trace period between CS and US in TFC causes more difficult TAL as previously shown in rats (Misane et al. 2005), and further supporting the idea of duration dependency in trace learning (Chowdhury et al. 2005; Misane et al. 2005).

Ablation of Island cells in MEC partially enhances L-TFC

To test the effect of the ablation of MECII Island cells on L-TFC, we bilaterally injected AAV₅-EF1 α -flex-taCasp3-TEVp into the MEC of either Wfs1-Cre mice (Casp⁺ group) or wild-type (WT) littermates (Casp⁻ group) as a control to induce Cre-dependent apoptosis in Island cells of the MEC. The genetically engineered procaspase 3 (pro-taCasp3) triggers cell-autonomous apoptosis by activation of the heterologous enzyme tobacco etch virus protease (TEVp) (Yang et al. 2013). At 4 wk after the injection of AAV₅-EF1 α -flex-taCasp3-TEVp into MECII, we found virtually no Wfs1⁺ (a marker for Island cells) cells in the MECII of the Casp⁺ group, while Wfs1⁻ neurons were seen to infiltrate the area without disturbance of the cortical laminar structure (Fig. 3A). The Casp⁻ control group maintained the Wfs1⁺ cell population that forms the Island cell clusters in the MECII (Fig. 3A). We subjected the Casp⁻ and Casp⁺ group to L-TFC 4 wk after AAV injection. In the conditioning session on day 1, the Casp⁺ group exhibited similar a freezing response to the control Casp⁻ group (two-way repeated measure [RM] ANOVA, effect of condition: $F_{(1,18)}=1.13$, $P>0.30$; effect of time: $F_{(41,738)}=75.6$, $P<0.001$; interaction: $F_{(41,738)}=0.98$, $P>0.51$) (Fig. 3B). In the testing session on day 2, however, while there was no difference in the freezing responses during either the baseline period or tone period between the Casp⁻ and Casp⁺ groups (unpaired t -test, base: $t_{18}=0.44$, $P>0.67$; tone: $t_{18}=0.56$, $P>0.58$) (Fig. 3C,D), the Casp⁺ group showed a significantly higher freezing response during the first minute post-tone period compared with the Casp⁻ group (unpaired t -test, $t_{18}=2.73$, $P<0.01$) (Fig. 3C,D). Together, these results suggest that the elimination of Island cells in MEC partially enhances L-TFC.

Chemogenetic inhibition of Island cell activity in MEC reduces L-TFC

To investigate the role of Island cell activity on L-TFC, we next examined chemogenetic neural activity inhibition using Designer Receptors Exclusively Activated by Designer Drugs (DREADDs) (Armbruster et al. 2007; Zhu et al. 2014; Roth 2016). First, we checked the proportion of hM4Di-mCherry-expressing cells in MEC of Wfs1-Cre mice injected with AAV₈-hSynI-DIO-hM4Di-mCherry to Wfs1-immunoreactive cells. Most of the mCherry-expressing cells in the MEC expressed Wfs1 (Wfs1/mCherry: $96.2\% \pm 0.7\%$, 339 cells from three mice) (Fig. 4A), as previously demonstrated (Kitamura et al. 2014). Then, we tested the efficacy of hM4Di inhibition in the Island cells of Wfs1-Cre mice that had been injected into the MEC with AAV₈-hSynI-DIO-hM4Di-mCherry (Krashes et al. 2011) using ex vivo patch clamp (Fig. 4B, C). Ten minutes after the application of 10 μ M clozapine-N-oxide (CNO) to patched Island cells, we observed increased rheobase

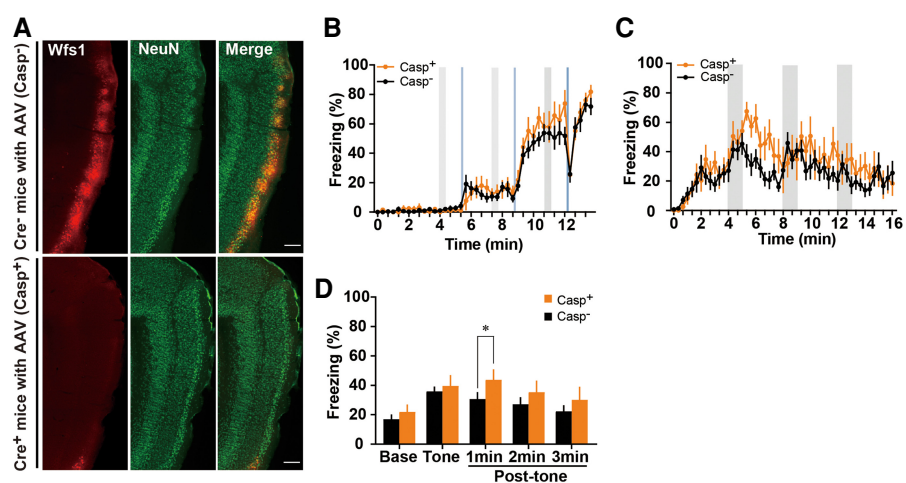


Figure 3. Effects of ablation of Island cells in the medial entorhinal cortex (MEC) on long trace fear conditioning (L-TFC). (A) Representative images in the MEC of Wfs1-Cre⁺ mice (bottom panels) and Wfs1-Cre⁻ littermates (top panels) at 4 wk after AAV-EF1 α -flex-taCasp3-TEVp injection. Scale bar, 200 μ m. (B) Time course of freezing responses in apoptosis-inducible Wfs1-Cre⁺ mice (Casp⁺ group, $n=8$) and Wfs1-Cre⁻ littermates (Casp⁻ group, $n=12$) during conditioning with 60-sec trace period on day 1 at 4 wk after the AAV injection. Gray and blue bars represent tone and shock, respectively. (C) Time course of freezing responses in both Casp⁺ and Casp⁻ groups during the test. Gray bars each indicate 60-sec tone representations. (D) The averaged freezing responses over the three bins during each tone period and that of the first 1-min, second, and third post-tone periods. Means \pm SEM. Two-way repeated measure (RM) analysis of variance (ANOVA) for B and C. (*) $P<0.05$ by unpaired t -test for D.

(paired t -test, $t_9=2.90$, $P<0.02$) (Fig. 4B) and reduced firing frequency at a 300 pA current pulse (paired t -test, $t_8=2.96$, $P<0.02$) (Fig. 4B), indicating a net reduction in neuronal excitability compared to the baseline levels without the presence of the DREADD agonist CNO in the bath solution. Interestingly, while the resting membrane potential (RMP) was quickly and significantly reduced from baseline RMP (3 min from CNO application, one sample t -test, $t_8=4.228$, $P<0.01$; 5 min from CNO application, one sample t -test, $t_8=2.540$, $P<0.05$), we observed a gradual rebound of the reduced RMP in a subset of Island cells (10 min from CNO application, one sample t -test, $t_8=2.132$, $P=0.065$) (Fig. 4C), contrary to what has been seen using chemogenetic techniques for neuronal inhibition at the tested dosage (10 μ M) of CNO in the hippocampus and hypothalamus (Krashes et al. 2011; Zhu et al. 2014), suggesting a robust mechanism may exist for the maintenance and balancing of the RMP in a subpopulation of Island cells.

Behavioral observation of the DREADDs' effects on L-TFC were performed using two groups of Wfs1-Cre mice; the hM4Di-mCherry-expressing (hM4Di-mCherry group) or mCherry-expressing (mCherry group), which had been injected with AAV₈-hSynI-DIO-hM4Di-mCherry or AAV₈-hSynI-DIO-mCherry, respectively, into the MEC. We administered the hM4Di-mCherry and mCherry groups CNO via intraperitoneal injection (4 mg/kg) 30 min before L-TFC. In the conditioning session on day 1, the hM4Di-mCherry group showed a similar freezing response to the control mCherry group (two-way RM ANOVA, effect of condition: $F_{(1,18)}=4.11$, $P>0.06$; effect of time: $F_{(41,738)}=73.3$, $P<0.001$; interaction: $F_{(41,738)}=1.45$, $P<0.04$) (Fig. 4D). In the testing session on day 2, the hM4Di-mCherry group showed a deficit in freezing responses during the tone period and the 1-, 2-, and 3-min post-tone periods compared with the mCherry group (unpaired t -test, tone: $t_{18}=2.62$, $P<0.02$; 1 min: $t_{18}=3.50$, $P<0.003$; 2 min: $t_{18}=2.37$, $P<0.03$; 3 min: $t_{18}=2.32$, $P<0.03$) (Fig. 4E,F). These results suggest that the chemogenetic manipulation of Island cell activity in the MEC impairs L-TFC in this condition.

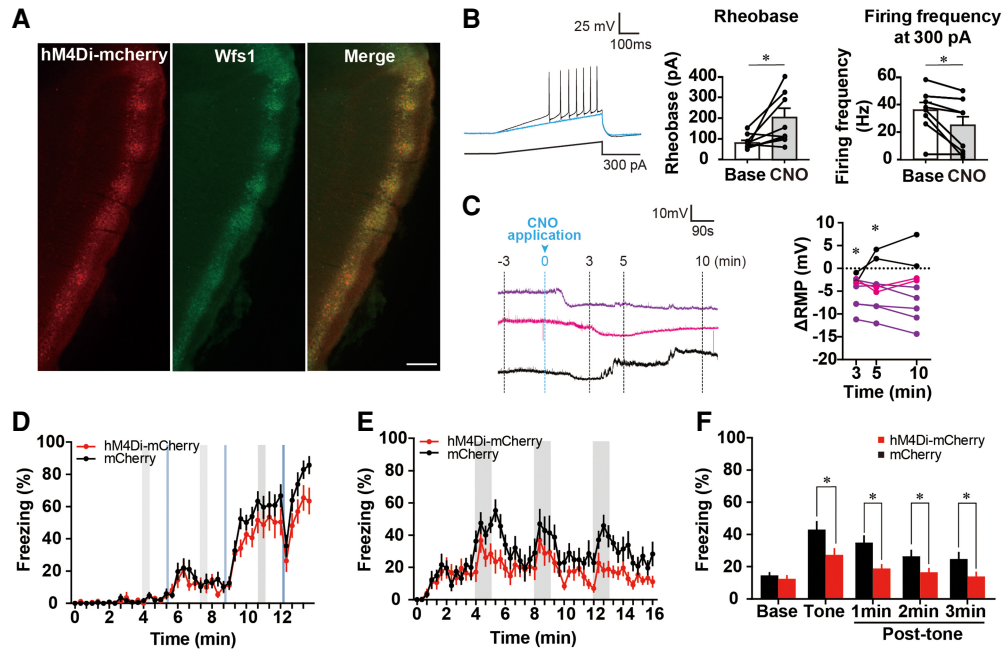


Figure 4. Effects of chemogenetic silencing of Island cell activity in the medial entorhinal cortex (MEC) during conditioning on long trace fear conditioning (L-TFC). (A) Representative images in the MEC of hM4Di-mCherry-expressing Wfs1-Cre mice. Scale bar, 200 μ m. (B) Changes in membrane excitability induced by clozapine-N-oxide (CNO) application. (Left panel) CNO reduces current needed to initiate action potentials (rheobase) assessed using a 500-sec, 300-pA ramping protocol before (black trace) and after (blue trace) CNO application. Line below depicts current ramp protocol. (Center panel) Application of CNO significantly increases the current required to initiate action potentials. (Right panel) the firing frequency of Island cells is significantly reduced at the same current stimulus level after CNO application. (C) Resting membrane potential reduction in Island cells measured patch clamp in tissue sections. Left panel shows three sample traces, which were dropping (purple), mildly rebounding (magenta), and strongly rebounding (black), depicting the change in resting membrane potential (RMP) following before and after CNO application (blue dashed line, time 0). Right panel shows the delta RMP following CNO application ($n=9$ cells across five animals). The color codes match the representative traces shown on left panel. (D) Time course of freezing responses in hM4Di-mCherry-expressing Wfs1-Cre mice (hM4Di-mCherry group; $n=10$) and mCherry-expressing mice (mCherry group; $n=10$) during conditioning with the 60-sec trace period on day 1. Gray and blue bars represent tone and shock, respectively. (E) Time course of freezing responses in both hM4Di-mCherry and mCherry group during the test. Gray bars indicate 60-sec tone representations each. (F) The averaged freezing responses over the three bins during each tone period and that of the first 1-min, second, and third post-tone periods. Means \pm SEM. Two-way repeated measure analysis of variance (RM ANOVA) for C. (*) $P < 0.05$ by unpaired t -test for F.

Optogenetic terminal inhibition of MECII Island cell synapses at dorsal hippocampal CA1 enhances L-TFC

To examine the role of Island cell inputs into dorsal HPC CA1 during the CS-US association period on L-TFC, we bilaterally injected either AAV₉-EF1 α -DIO-eArchT3.0-enhanced yellow fluorescent protein (eYFP) (Mattis et al. 2011) or AAV₉-EF1 α -DIO-eYFP as a control into the MEC of Wfs1-Cre mice, bilaterally implanted optic fibers into dorsal HPC CA1, and then subjected them to L-TFC with green light illumination (561 nm) only during the CS-US association periods (total 82 sec; 20 sec [tone]+60 sec [trace]+2 sec [shock]) (Fig. 5A). We have previously confirmed that the optogenetic terminal inhibition of Island cells at dorsal HPC CA1 increases the spiking activity in CA1 pyramidal cells (Kitamura et al. 2014), indicating that the optogenetic terminal inhibition suppresses the feed-forward inhibition of HPC CA1 pyramidal cells driven by Island cell inputs. In the conditioning session on day 1, eArchT3.0-eYFP-expressing Wfs1-Cre mice (ArchT-eYFP group) exhibited

higher freezing responses compared with the control eYFP-expressing ones (eYFP group, two-way RM ANOVA, effect of condition: $F_{(1,16)}=8.16$, $P < 0.01$; effect of time: $F_{(41,656)}=41.1$, $P < 0.001$; interaction: $F_{(41,656)}=2.28$, $P < 0.001$) (Fig. 5A). In the testing session on

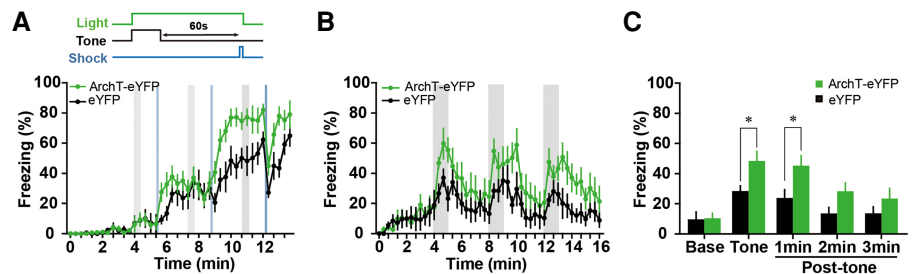


Figure 5. Effects of optogenetic terminal inhibition of Island cells in medial entorhinal cortex (MEC) at dorsal hippocampal CA1 during conditioned stimulus (CS)-unconditioned stimulus (US) pairing periods on long trace fear conditioning (L-TFC). (A) Time course of freezing responses in eArchT3.0-enhanced yellow fluorescent protein (eYFP)-expressing Wfs1-Cre mice (ArchT-eYFP group, $n=9$) and control eYFP-expressing mice (eYFP group, $n=9$) during conditioning with a 60-sec trace period on day 1. Gray and blue bars represent tone and shock, respectively. The averaged freezing response in ArchT-eYFP group was different from that in the eYFP group. (B) Time course of freezing responses in both ArchT-eYFP and eYFP groups during the testing protocol. Gray bars indicate 60-sec tone representations. (C) The averaged freezing responses over the three bins during each tone period and that of the first, second, and third 1-min post-tone periods. Means \pm SEM. Two-way repeated measure analysis of variance (RM ANOVA) for A. (*) $P < 0.05$ by unpaired t -test for C.

day 2, the ArchT group showed higher freezing responses during the tone period and post-tone for the first 1-min period compared with those in the eYFP group (unpaired *t*-test, tone: $t_{16} = 2.74$, $P < 0.02$; 1 min: $t_{16} = 2.46$, $P < 0.03$) (Fig. 5B,C). Previous work demonstrates that Island cell inhibition with a short trace period (20 sec) has a similar boosting effect on freezing levels to what we see here with a 60-sec trace period, but that Island cell activity has no effect on delay fear conditioning, which does not have a temporal gap between CS and US (Kitamura et al. 2014). These results, combined with previous reports, suggest that the optogenetic terminal inhibition of Island cells in the MEC at dorsal HPC CA1 during the CS–US association periods enhances L-TFC.

Discussion

Previously, our group has established that Island cells are involved in the modulation of TFC with a 20-sec trace period, but not delay fear conditioning (Kitamura et al. 2014) or contextual fear conditioning (Kitamura et al. 2015b), indicating a specificity of involvement in TAL, rather than fear conditioning in general. In this study, by using an L-TFC protocol with a 60-sec trace period (Fig. 2), we examined the regulatory role of Island cells on TFC with a long temporal gap between events. We found that the elimination of Island cells in the MEC partially enhanced L-TFC (Fig. 3), chemogenetic manipulation of Island cells causes differential levels of efficacy and leads to a circuit imbalance that disrupts L-TFC (Fig. 4), and, finally, that optogenetic terminal inactivation of Island cells at dorsal HPC CA1 during CS–US association periods enhanced L-TFC (Fig. 5). Of particular interest was the comparison between local synaptic inactivation (Fig. 5) and gross circuit inhibition, respectively (Figs. 3 and 4). These experiments suggest that Island cells in MECII regulate L-TFC and the temporal inhibition of Island cell inputs into HPC CA1 only during CS–US association would be required for sufficient artificial facilitation of L-TFC.

Ablation of Island cells in the MEC using an inducible caspase construct (Yang et al. 2013) led to a significant increase of the freezing response in L-TFC (Fig. 3D), similar to the result of the optogenetic terminal inhibition of Island cells at HPC CA1 (Fig. 5C,D). Despite the similarity in the enhanced freezing response during the 1-min post-tone period, we observed no difference during the tone period in the Casp⁺ group compared with the Casp⁻ group (Fig. 3D). While it may be possible that the lack of response during the tone period overall may be due to insufficient acquisition due to the prolonged absence of Island cells in the MEC, we also speculate that the Casp⁺ group might remember the timing of the footshock delivery. Given that the animals have had 4 wk between injection of the caspase virus and experimentation, the elimination of Island cells could cause compensation in the EC networks, which could lead to a partial restoration of function that is less amenable to modulation (Jinde et al. 2012; Couey et al. 2013; Zelikowsky et al. 2013; Ohara et al. 2019). Since the lateral entorhinal cortex (LEC), in particular, has a role in trace eyeblink conditioning (Takehara-Nishiuchi et al. 2011; Morrissey et al. 2012; Pilkiw et al. 2017; Marks et al. 2020) and other forms of temporal learning (Chao et al. 2016), we suspect that the function may be partially picked up by the Wfs⁺ Islands of the LECII, which were unaffected by our targeted ablation, and also project to the SL of CA1 (Kitamura et al. 2014). With the overlap in anatomical connectivity and local cytoarchitecture between LEC and MEC, it seems reasonable that there could be compensation in one segment of ECII when the other is compromised, and that the functional separation between MEC and LEC is not as discrete as assumed (Save and Sargolini 2017).

Previously it was determined that reducing neural input strength from Island cells or increasing MECIII input enhanced

TFC with weaker external stimuli in the 20-sec TFC paradigm (Kitamura et al. 2014). In this study, we showed that optogenetic terminal inhibition of Island cells in the MEC at dorsal HPC CA1 resulted in the greater freezing response in L-TFC, compared with the eYFP control group (Fig. 5B,C). Our experiment disinhibited the processed input from MECIII (Kitamura et al. 2014), leaving the rest of the HPC processing apparatus largely intact for fine-tuned processing of an artificially boosted temporal signal (McEchron et al. 2003; Pastalkova et al. 2008; MacDonald et al. 2011; Pelkey et al. 2017; Marks et al. 2019; Zhang et al. 2019; Zhou et al. 2020). Therefore, this experiment suggests that the Island cells in the MEC exert control over the allowed length of time between events that can become associated across time. Considering the extension of duration gained by reduced synaptic activity onto the inhibitory interneurons in SL of the dorsal hippocampus, it is reasonable to suppose that under normal conditions the strength or number of activated Island cells could vary, exerting a stronger or weaker control over the temporal signal and, therefore, which events become associated. Our study suggests that Island cells control L-TFC as well as TAL with low impact/salience events (e.g., reduced footshock intensity) for optimal adaptive memory formation by regulating the MECIII inputs into the HPC CA1, which would be driven by tone-induced persistent activity (Yoshida et al. 2008; Kitamura et al. 2014).

We observed that the hM4Di-mCherry-expressing mice showed a reduction of the freezing response in L-TFC compared with the mCherry control group (Fig. 4) following exposure to CNO. This result would appear to be indicative of the overall inhibition of Island cells, but yet appears contrary to our observations of increased freezing following optogenetic terminal inhibition of Island cells in the hippocampus (Fig. 5), and the extensive ablation of Island cells (Fig. 3); however, we believe this result points to a more dynamic process underlying the activity of Island cells in TAL. Our confirmatory process of patch clamping Island cells to verify function of the hM4Di construct yielded a surprising observation (Fig. 4B,C) that some Island cells showed a tendency to rebound after an initial hyperpolarization in response to CNO (Fig. 4C). In addition, we observed a wide spread of CNO effects on excitability (Fig. 4C), although the overall effect was clearly inhibitory. It is possible the population of Island cells may be more heterogenous than previously understood (Berggaard et al. 2018; Grosser et al. 2021), perhaps with differential expression of voltage-gated ion channels. Within the population of Island cells in the MEC, differential expression of GABA receptor $\alpha 3$ has been observed and hypothesized to generate differential activity patterns (Fuchs et al. 2016; Berggaard et al. 2018; Grosser et al. 2021), so it is not unlikely that other differences may exist, and distinct functional subtypes of Island cells have yet to be defined. Furthermore, although the overall effect of the DREADDs is inhibitory, it does not result in a complete abolition of firing (as with optogenetic inhibition), merely a reduction. An unbalanced reduction, or differential levels of G_i activity across the total population would result in the scrambling of a normally coherent signal. This suggests that our result is not simply dependent on the overall inhibitory effect we observed, but also that the pattern of Island cell activity may be important, and that even a subtle unbalancing or shifting of the standard activity patterns of a subset of Island cells can have a drastic effect on the capability of TAL (Kitamura et al. 2014), essentially taking a well-coordinated signal that would normally result in TAL and scrambling it into a nonsense signal, resulting in the observed decrease of freezing rather than an increase as observed in the optogenetic terminal inhibition experiment and Island cell ablation experiment. Future studies focused on the diversity of single-cell responses of Island cells during TFC, the existence of functional subsets within the broad class of Island cells, and the generation of a coherent signal/decoding of the information

contained in the Island cell signal might be called for in light of these findings.

In this study, we have used multiple techniques to identify the role of Island cells on L-TFC. As a methodological discussion, we note the advantage/disadvantages of each approach based on our experimental results. Optogenetic approaches allow for the temporally precise terminal inhibition, but are better suited to small subregions of the brain rather than whole-system inhibition. In our case, we successfully used targeted light illumination to silence Island cell axons, since Island cells specifically project to SL in HPC CA1 (Fig. 1). Chemogenetic neural manipulation allows whole-system inhibition of a cell type and all its projections, but causes a partial, rather than total inhibition of neural firing by biasing cells toward a hyperpolarized state. However, depending on neural cell type, it may cause artificial generation of an aberrant/nonsense signal, as we observed in Figure 4. Finally, cell type-specific ablation allows for complete elimination of the target population, but leaves time for systemic compensation to attempt to restore a homeostatic balance in the brain prior to behavioral testing. Although each of these techniques is powerful, the choice of which technique to use depends on the experimental question. Here, using these techniques on the same circuit system yielded differing results that on the surface appear to be contradictory; however, each provides a unique insight into the system that is not achievable with the others.

We have demonstrated through multiple complimentary techniques that the Island cells of MECII regulate the linking of temporally discontinuous events in terms of weaker impact of events or longer duration of temporal gap between events. The identity of the driving factors that regulate Island cell activity for this linking function by MECII is still unclear. It has been suggested that the individual Island clusters may have unique processing capabilities, but to what degree remains unclear (Ray et al. 2014; Fuchs et al. 2016). A recent report has suggested a gradient of parvalbumin⁺ interneuron activity along the dorsal ventral axis of the Island cell distribution, implying differential processing along this axis (Grosser et al. 2021). It is also not clear yet what the specific inputs to the Island cells are and what information is initiating their temporal-gating activity. One possibility is that the medial prefrontal cortex (mPFC), which has been shown to play a role in the retention of the conditioned response in trace eyeblink conditioning (Volle et al. 2016; Jarovi et al. 2018) as well as temporal order memory (Naya et al. 2017), may be involved in this gating, sending information about the salience of the objects involved in individual events, determining what degree of threat or benefit is involved, and therefore the relevance between any two events due to its involvement in stimulus and mnemonic discrimination, as well as working memory (Dolleman-Van Der Weel and Witter 1996; Weible et al. 2000; Chiba et al. 2001; Knight et al. 2004; Gilmartin and McEchorn 2005; Guimaraes et al. 2011; Johnson et al. 2021). The involvement of amygdala seems likely given the importance of emotional valence in memory and threat discrimination, and the fact that the amygdala can facilitate integration of information transmitted by mPFC inputs to perirhinal cortex into MEC layer II/III (Phillips and LeDoux 1992; Kajiwara et al. 2003; Paz et al. 2006; Wahlstrom et al. 2018). Understanding what the driving factors underlying this process are will give greater insight into TAL.

In this study, we have demonstrated that the Island cells in the MEC regulate the duration of the temporal gap between events in TFC. By reducing and modulating the input from Island cells to SL-INs, we were able to artificially associate or separate two temporally discontinuous events during L-TFC. These findings open new avenues for investigation into the driving factors of the external control of temporal association and the formation of larger episodic memories.

Materials and Methods

Animals

WT male C57BL/6J mice purchased from Jackson laboratory (between 12 and 20 wk old) and Wfs-1 Cre male and female mice (RBRC03751; between 4 wk and 20 wk old) were group housed with littermates (two to five mice per cage) in a 12-h (6 a.m.–6 p.m.) light–dark cycle, with food and water available ad libitum. All experiments were conducted during the light cycle. Mice were randomly assigned to experimental conditions. All animal procedures were conformed to National Institutes of Health (NIH) and institutional guidelines and approved by the University of Texas (UT) Southwestern Institutional Animal Care and Use Committee (IACUC).

Stereotaxic surgery and virus microinjection

All animal aseptic surgeries were conducted with a stereotaxic frame (David Kopf Instruments) and followed NIH and UT Southwestern IACUC guidelines. Mice were anesthetized with 4% isoflurane for induction and with 1%–2% isoflurane for maintenance of anesthesia during surgery. A small amount of 2% lidocaine was placed on and under the skin as a topical analgesic and a small hole was drilled above each injection site. Microinjections were completed with a 10- μ L Hamilton microsyringe and a glass micropipette filled with mineral oil and attached to a microsyringe pump (World Precision Instruments) with viral injections performed at a rate of 2 nL/sec. Coordinates are given relative to Bregma (in millimeters). The EC was targeted at AP: -4.85 , ML: ± 3.45 , DV: -3.30 . The micropipette was allowed to remain in place for 5 min following each injection to avoid backflow of the viral solution. For optogenetic experiments, after injection, a Doric patchcord optical fiber (200- μ m core diameter) was placed above the SL-layer in the CA1 region (Bregma: AP: -2.20 , ML: ± 1.5 , DV: -1.30) as described previously (Kitamura et al. 2014). At the end of surgery, mice were given 0.9% sterile saline and meloxicam (2 mg/kg) as an analgesic, placed on a heating pad until fully recovered from the anesthesia, and were allowed to recover for a minimum of 3 d before returning to group housing with cagemates. After finishing all behavioral procedures, we performed histology to verify the target sites and expression of AAV injection.

Trace fear conditioning

TFC was performed on WT or Wfs1-Cre male mice aged between 12 and 20 wk during the light cycle with minor modifications of the method as described previously (Kitamura et al. 2014). All animals were handled 5 min a day for five consecutive days prior to experimentation. The protocol of fear conditioning in WT mice with 20- or 60-sec trace periods was performed in a soundproof fear conditioning chamber (Med Associates). On day 1, mice were placed in context A (dim white light, white plastic semicircular board inserted into the chamber scented with 1% acetic acid) and allowed to explore for 240 sec, at which point a 20-sec tone (85 dB, 5 kHz) was played as conditioned stimulus (CS) followed by either a 20- or 60-sec trace, and then a 2-sec, 1.0-mA footshock as unconditioned stimulus (US). This was repeated two more times, starting at 402 and 564 sec or 442 and 604 sec, respectively. Mice remained in the conditioning chamber in each protocol for a total of 706 or 826 sec, respectively. On day 2, mice were placed in context B (dim red light, black plexiglass triangle inserted into the chamber and a white plastic board on the grid, unscented) and allowed to explore for 240 sec, at which the same 20- or 60-sec tone was played, followed by a 180-sec post-tone period. This was repeated two more times and mice were then returned to their home cage after 960 sec in the chamber.

In the optogenetic experiment, Wfs1-Cre mice were bilaterally inoculated with AAV₉-EF1a-DIO-eArchT3.0-eYFP (UNC Vector Core, 1.6×10^{12} gc/mL) or AAV₉-EF1a-DIO-eYFP (UNC Vector Core, 1.2×10^{12} gc/mL) at AP: -4.85 , ML: ± 3.45 , DV: -3.30 at a volume of 200 nL/site. Mice were allowed to recover for 2 wk before returning to group housing with cagemates. One week after the group housing, mice were subjected to behavior experiments, the optical fiber implant was connected to a 561-nm laser controlled

by a function generator. Mice were then placed in context A and allowed to explore for 180 sec, at which point a 20-sec tone (75 dB, 2000 Hz) was played, followed by a 60-sec trace, and then a 2-sec, 0.75-mA footshock. This was repeated two more times, starting at 442 and 604 sec. During the CS-US pairing periods (82 sec) (Fig. 5A), mice received green light stimulation (15 mW, both hemispheres). Mice remained in the conditioning chamber for a total of 826 sec. On day 2, mice were placed in context B and allowed to explore for 180 sec, at which point the same 60-sec tone was played, followed by 180 sec of post-tone period. This was repeated two more times and mice were then returned after 880 or 960 sec in the chamber, respectively.

In the chemogenetic experiments, Wfs1-Cre mice were bilaterally inoculated with AAV₈-hSyn-DIO-hM4Di-mCherry (2.9×10^{13} gc/mL; Addgene) or AAV₈-hSyn-DIO-mCherry (2.3×10^{13} gc/mL; Addgene) at AP: -4.85, ML: ± 3.45 , DV: -3.30 at a volume of 200 nL/side. Mice were allowed to recover for 2 wk before returning to group housing with cagemates. One week after group rehousing, mice were subjected to behavioral experiments or electrophysiological experiments. We performed the same behavioral procedure followed as the long trace (60-sec) TFC protocol described above. At 30 min prior to the conditioning session (Fig. 4C), these Wfs1-Cre mice were intraperitoneally injected with CNO at dose of 4 mg/kg in sterile saline (Enzo).

In the induced-apoptosis experiment, Wfs1-Cre mice and WT littermates were bilaterally inoculated with AAV₅-EF1a-flex-taCasp3-TEVp (4.0×10^{12} gc/mL; Addgene) at AP: -4.85, ML: ± 3.45 , DV: -3.30 at a volume of 300 nL/side. Mice were allowed to recover for 2 wk before returning to group housing with cagemates. Two weeks after the group rehousing, we performed the same L-TFC protocol described above at 4 wk after the surgery. All behavioral experiments were performed by a researcher blind to experimental conditions.

Immunohistochemistry

Mice were deeply anesthetized with a ketamine (75 mg/kg)/dexametomidine (1 mg/kg) cocktail by intraperitoneal injection and perfused transcardially with 4% paraformaldehyde (PFA) in phosphate-buffered saline (PBS). Brains were removed and post-fixed in 4% PFA in PBS for 24 h at 4°C and then sliced sagittally using a vibratome (Leica VT100S) to a thickness of 50 μ m. For immunohistochemistry (IHC), tissue sections were blocked in 0.4% Triton-X PBS (PBS-T) with 10% normal goat serum (NGS) for 1 h at room temperature. Primary antibodies were added to PBS-T with 10% NGS and then the sections were incubated on a shaker overnight at 4°C. Primary antibodies used for immunostaining were as follows: rabbit anti-Wfs1 (1:1000; Proteintech Group, Inc. 11558-1-AP) and chicken anti-NeuN (1:1000; Millipore Sigma ABN91). Sections were washed with PBS three times for 10 min each, followed by incubation for 2–3 h at room temperature with secondary antibody conjugated AlexaFluor488, AlexaFluor546 (1:500; Thermo Fisher Scientific) in PBS-T with 10% NGS. Following three additional washes for 10 min in PBS and sections mounted in VectaShield medium (Vector Laboratories) on glass slides. Some sections were counterstained with DAPI (1:1000; Thermo Fisher Scientific). Fluorescence images were taken with a Zeiss Axio Imager M2 microscope using the 10 \times objective or with a Zeiss LSM800 Airyscan using the 25 \times objective. Images were processed using Zen Blue software (Zeiss).

Ex vivo electrophysiology to verify inhibitory DREADD efficacy in Wfs1⁺ Island cells

Mice were anesthetized with 4% gaseous isoflurane, and transcardially perfused with calcium free sucrose cutting media (3 mM KCl, 4.12 mM MgSO₄, 1.2 mM NaH₂PO₄, 206 mM sucrose, 25 mM NaHCO₃, 25 mM glucose) held at 1°C–3°C and bubbled with a 5% CO₂ balanced-oxygen mix (Airgas). Following perfusion, brains were rapidly removed, halved along the sagittal sulcus, and then cut along the sagittal plane in 250- μ m sections from the lateral surface moving medially. Cutting was done using a Leica VT1000 S vibratome (Leica Biosystems). Brains were submerged

in oxygenated, calcium-free sucrose-supplemented cutting media at 1°C–3°C for the cutting process. Slices were moved to a custom beaker insert containing a nylon mesh and submerged in oxygenated extracellular recording media (3 mM KCl, 1.2 mM CaCl₂, 1.2 mM MgSO₄, 1.2 mM NaH₂PO₄, 125 mM NaCl, 25 mM NaHCO₃, 25 mM glucose) at 36°C within a water bath for 30 min. The beaker was removed from the bath and slices allowed to rest for 30 min before recording. The slices were maintained at room temperature until recordings began.

During recordings, tissue sections were constantly perfused with oxygenated extracellular recording media heated to 30°C–34°C using an in-line heater (Warner Instruments) driven by an external temperature control unit (Warner Instruments). The EC was visualized at 2.5 \times on a Zeiss Axio Examiner A1 microscope. Magnification was switched to 63 \times (fluid immersion objective) to visualize Island cells in ECII. Wfs1⁺ cells were excited using the X-Cite Xylis (Excelitas) LED system with a green filter cube to excite the associated mCherry construct for cell-specific targeting prior to patching. Pipettes for whole-cell patch clamp were pulled (Narishige) from borosilicate glass tubes (World Precision Instruments) to a resistance of 3–7 M Ω . Patch pipettes were filled with intracellular recording solution containing 135 mM KMeSO₄, 10 mM HEPES, 2 mM MgATP, 0.1 mM NaGTP, 8 mM NaCl, 0.1 mM BAPTA₄, 0.2% biocytin (pH 7.25). Recordings were made using a MultiClamp 700B amplifier (Molecular Devices), and digitized using a Digidata 1550B digitizer. Recordings and analysis were performed using Clampex/Clampfit 11.2 software (Molecular Devices) on a Microsoft computer. Membrane potentials were recorded before, during, and after a ramp protocol (0 to 300 pA over 500 msec), and in a current step protocol (25 pA current injections from -100 pA to 400 pA, 500 msec each with 800 msec total between). In two cases, the current ramp did not induce firing at 300 pA, and the maximum current injection was increased to 500 pA over 800 msec. After baseline recordings were obtained, ongoing passive recording of the membrane potential was engaged while 10 μ M CNO (HelloBio) was added into the extracellular media. A timestamp was made in the recording when CNO was added to the tissue chamber, 3 min after the recording began. This 3-min period is used as the baseline measurement. The recording was ended 10 min after the timestamp, and the ramp and current step protocols were repeated. Recordings were acquired with a lowpass filter at 4 kHz, and a sampling rate of 10 kHz at 1 \times gain.

All electrophysiological data was filtered using the Chebyshev method at 1200 Hz prior to analysis. Rheobase was determined using the current ramp protocol to identify the current level at which cells began firing. Change in membrane potential was measured as the difference in membrane potential between the timestamp and the 3-, 5-, and 10-min mark. Baseline drift was corrected from the slope of the pre-CNO application period.

Statistics

Calculated statistics of all data are presented as means \pm SEM. Experimenters were blinded to conditions of experiments during data acquisition and analysis. The experimental designs were counterbalanced. Statistical analyses were performed using GraphPad Prism 8 software. Physiological assessments were analyzed using paired *t*-tests for within subject measurements of rheobase and firing frequency. Assessments of RMP reduction were analyzed using one sample *t*-tests relative a nonchanging theoretical baseline. For behavioral experiments, comparisons of data between two groups were analyzed with two-tailed unpaired *t*-test, and multiple-group comparisons were assessed using two-way RM ANOVA when applicable, followed by Bonferroni's post hoc test. Using by paired *t*-tests for within subject measurements of averaged freezing percent between baseline and tone. All statistical tests assumed an α level of 0.05. For all figures, * = $P < 0.05$.

Acknowledgments

This work was supported by grants from Endowed Scholar Program to T.K., Brain Research Foundation to T.K. (BRFSG-2018-04),

Faculty Science and Technology Acquisition and Retention Program to T.K., the Brain & Behavior Research Foundation to T.K. (26391) and J.Y. (28801), the Whitehall Foundation to T.K. (2019-05-38), National Institute of Mental Health to T.K. (R01MH120134), and W.D.M. (F32MH122082), Daiichi Sankyo Foundation of Life Science to J.Y., the Uehara Memorial Foundation to J.Y., Japan Society for the Promotion of Science to N.Y. (201860573) and Human Frontier Science Program to T.K. (RGY0072/2018).

References

- Alonso A, Klink R. 1993. Differential electroresponsiveness of stellate and pyramidal-like cells of medial entorhinal cortex layer II. *J Neurophysiol* **70**: 128–143. doi:10.1152/jn.1993.70.1.128
- Amaral D, Lavenex P. 2007. Hippocampal neuroanatomy. In *The hippocampus book* (ed. Anderson P, Morris R, Amaral D, Bliss T, O'Keefe J), pp. 37–109. Oxford University Press, Oxford.
- Amaral DG, Witter MP. 1995. The three-dimensional organization of the hippocampal formation: a review of anatomical data. *Neuroscience* **31**: 571–591. doi:10.1016/0306-4522(89)90424-7
- Armbruster BN, Li X, Pausch MH, Herlitze S, Roth BL. 2007. Evolving the lock to fit the key to create a family of G protein-coupled receptors potentially activated by an inert ligand. *Proc Natl Acad Sci* **104**: 5163–5168. doi:10.1073/pnas.0700293104
- Berggaard N, Seifn, van der Want JLL, Swinny JD. 2018. Spatiotemporal distribution of GABA_A receptor subunits within layer II of mouse medial entorhinal cortex: implications for grid cell excitability. *Front Neuroanat* **12**: 46. doi:10.3389/fnana.2018.00046
- Buchel C, Dolan RJ. 2000. Classical fear conditioning in functional neuroimaging. *Curr Opin Neurobiol* **10**: 219–223. doi:10.1016/S0959-4388(00)00078-7
- Chao OY, Huston JP, Li JS, Wang AL, de Souza Silva MA. 2016. The medial prefrontal cortex-lateral entorhinal cortex circuit is essential for episodic-like memory and associative object-recognition. *Hippocampus* **26**: 633–645. doi:10.1002/hipo.22547
- Chiba T, Kayahara T, Nakano K. 2001. Efferent projections of infralimbic and prelimbic areas of the medial prefrontal cortex in the Japanese monkey, *Macaca fuscata*. *Brain Res* **888**: 83–101. doi:10.1016/S0006-8993(00)03013-4
- Chowdhury N, Quinn JJ, Fanselow MS. 2005. Dorsal hippocampus involvement in trace fear conditioning with long, but not short, trace intervals in mice. *Behav Neurosci* **119**: 1396–1402. doi:10.1037/0735-7044.119.5.1396
- Clark RE, Squire LR. 1998. Classical conditioning and brain systems: the role of awareness. *Science* **280**: 77–81. doi:10.1126/science.280.5360.77
- Couey JJ, Witoelar A, Zhang SJ, Zheng K, Ye J, Dunn B, Czajkowski R, Moser MB, Moser EI, Roudi Y, et al. 2013. Recurrent inhibitory circuitry as a mechanism for grid formation. *Nat Neurosci* **16**: 318–324. doi:10.1038/nn.3310
- Crestani F, Keist R, Fritschy JM, Benke D, Vogt K, Prut L, Bluthmann H, Mohler H, Rudolph U. 2002. Trace fear conditioning involves hippocampal $\alpha 5$ GABA_A receptors. *Proc Natl Acad Sci* **99**: 8980–8985. doi:10.1073/pnas.142288699
- Delgado MR, Olsson A, Phelps EA. 2006. Extending animal models of fear conditioning to humans. *Biol Psychol* **73**: 39–48. doi:10.1016/j.biopsycho.2006.01.006
- Dolleman-Van Der Weel MJ, Witter MP. 1996. Projections from the nucleus reuniens thalami to the entorhinal cortex, hippocampal field CA1, and the subiculum in the rat arise from different populations of neurons. *J Comp Neurol* **364**: 637–650. doi:10.1002/(SICI)1096-9861(19960122)364:4<637::AID-CNE3>3.0.CO;2-4
- Eichenbaum H. 2000. A cortical-hippocampal system for declarative memory. *Nat Rev Neurosci* **1**: 41–50. doi:10.1038/35036213
- Esclassan F, Coutureau E, Di Scala G, Marchand AR. 2009. A cholinergic-dependent role for the entorhinal cortex in trace fear conditioning. *J Neurosci* **29**: 8087–8093. doi:10.1523/JNEUROSCI.0543-09.2009
- Fendt M, Fanselow MS. 1999. The neuroanatomical and neurochemical basis of conditioned fear. *Neurosci Biobehav Rev* **23**: 743–760. doi:10.1016/S0149-7634(99)00016-0
- Fuchs EC, Neitz A, Pinna R, Melzer S, Caputi A, Monyer H. 2016. Local and distant input controlling excitation in layer II of the medial entorhinal cortex. *Neuron* **89**: 194–208. doi:10.1016/j.neuron.2015.11.029
- Fujimaru Y, Kosaka T. 1996. The distribution of two calcium binding proteins, calbindin D-28K and parvalbumin, in the entorhinal cortex of the adult mouse. *Neurosci Res* **24**: 329–343. doi:10.1016/0168-0102(95)01008-4
- Gilmartin MR, Helmstetter FJ. 2010. Trace and contextual fear conditioning require neural activity and NMDA receptor-dependent transmission in the medial prefrontal cortex. *Learn Mem* **17**: 289–296. doi:10.1101/lm.1597410
- Gilmartin MR, McEchron MD. 2005. Single neurons in the medial prefrontal cortex of the rat exhibit tonic and phasic coding during trace fear conditioning. *Behav Neurosci* **119**: 1496–1510. doi:10.1037/0735-7044.119.6.1496
- Grosser S, Barreda FJ, Beed P, Schmitz D, Booker SA, Vida I. 2021. Parvalbumin interneurons are differentially connected to principal cells in inhibitory feedback microcircuits along the dorsoventral axis of the medial entorhinal cortex. *eNeuro* **8**: ENEURO.0354-20.2020. doi:10.1523/ENEURO.0354-20.2020
- Guimaraes M, Gregorio A, Cruz A, Guyon N, Moita MA. 2011. Time determines the neural circuit underlying associative fear learning. *Front Behav Neurosci* **5**: 89. doi:10.3389/fnbeh.2011.00089
- Hales JB, Vincze JL, Reitz NT, Ocampo AC, Leutgeb S, Clark RE. 2018. Recent and remote retrograde memory deficit in rats with medial entorhinal cortex lesions. *Neurobiol Learn Mem* **155**: 157–163. doi:10.1016/j.nlm.2018.07.013
- Heys JG, Wu Z, Allegra Mascaro AL, Dombeck DA. 2020. Inactivation of the medial entorhinal cortex selectively disrupts learning of interval timing. *Cell Rep* **32**: 108163. doi:10.1016/j.celrep.2020.108163
- Huerta PT, Sun LD, Wilson MA, Tonegawa S. 2000. Formation of temporal memory requires NMDA receptors within CA1 pyramidal neurons. *Neuron* **25**: 473–480. doi:10.1016/S0896-6273(00)80909-5
- Jarovi J, Volle J, Yu X, Guan L, Takehara-Nishiuchi K. 2018. Prefrontal theta oscillations promote selective encoding of behaviorally relevant events. *eNeuro* **5**: ENEURO.0407-18.2018. doi:10.1523/ENEURO.0407-18.2018
- Jinde S, Ziros V, Jiang Z, Nakao K, Pickel J, Kohno K, Belforte JE, Nakazawa K. 2012. Hilar mossy cell degeneration causes transient dentate granule cell hyperexcitability and impaired pattern separation. *Neuron* **76**: 1189–1200. doi:10.1016/j.neuron.2012.10.036
- Johnson SA, Zequeira S, Turner SM, Maurer AP, Bizon JL, Burke SN. 2021. Rodent mnemonic similarity task performance requires the prefrontal cortex. *Hippocampus* **31**: 701–716. doi:10.1002/hipo.23316
- Kajiwara R, Takashima I, Mimura Y, Witter MP, Iijima T. 2003. Amygdala input promotes spread of excitatory neural activity from perirhinal cortex to the entorhinal-hippocampal circuit. *J Neurophysiol* **89**: 2176–2184. doi:10.1152/jn.01033.2002
- Kawano J, Fujinaga R, Yamamoto-Hanada K, Oka Y, Tanizawa Y, Shinoda K. 2009. Wolfram syndrome 1 (Wfs1) mRNA expression in the normal mouse brain during postnatal development. *Neurosci Res* **64**: 213–230. doi:10.1016/j.neures.2009.03.005
- Kim JJ, Jung MW. 2006. Neural circuits and mechanisms involved in Pavlovian fear conditioning: a critical review. *Neurosci Biobehav Rev* **30**: 188–202. doi:10.1016/j.neubiorev.2005.06.005
- Kitamura T. 2017. Driving and regulating temporal association learning coordinated by entorhinal-hippocampal network. *Neurosci Res* **121**: 1–6. doi:10.1016/j.neures.2017.04.005
- Kitamura T, Pignatelli M, Suh J, Kohara K, Yoshiki A, Abe K, Tonegawa S. 2014. Island cells control temporal association memory. *Science* **343**: 896–901. doi:10.1126/science.1244634
- Kitamura T, Macdonald CJ, Tonegawa S. 2015a. Entorhinal-hippocampal neuronal circuits bridge temporally discontinuous events. *Learn Mem* **22**: 438–443. doi:10.1101/lm.038687.115
- Kitamura T, Sun C, Martin J, Kitch LJ, Schnitzler MJ, Tonegawa S. 2015b. Entorhinal cortical ocean cells encode specific contexts and drive context-specific fear memory. *Neuron* **87**: 1317–1331. doi:10.1016/j.neuron.2015.08.036
- Kitamura T, Ogawa SK, Roy DS, Okuyama T, Morrissey MD, Smith LM, Redondo RL, Tonegawa S. 2017. Engrams and circuits crucial for systems consolidation of a memory. *Science* **356**: 73–78. doi:10.1126/science.aam6808
- Klink R, Alonso A. 1997. Morphological characteristics of layer II projection neurons in the rat medial entorhinal cortex. *Hippocampus* **7**: 571–583. doi:10.1002/(SICI)1098-1063(1997)7:5<571::AID-HIPO12>3.0.CO;2-Y
- Knight DC, Cheng DT, Smith CN, Stein EA, Helmstetter FJ. 2004. Neural substrates mediating human delay and trace fear conditioning. *J Neurosci* **24**: 218–228. doi:10.1523/JNEUROSCI.0433-03.2004
- Kohara K, Pignatelli M, Rivest AJ, Jung HY, Kitamura T, Suh J, Frank D, Kajikawa K, Mise N, Obata Y, et al. 2014. Cell type-specific genetic and optogenetic tools reveal hippocampal CA2 circuits. *Nat Neurosci* **17**: 269–279. doi:10.1038/nn.3614
- Krashes MJ, Koda S, Ye C, Rogan SC, Adams AC, Cusher DS, Maratos-Flier E, Roth BL, Lowell BB. 2011. Rapid, reversible activation of AgRP neurons drives feeding behavior in mice. *J Clin Invest* **121**: 1424–1428. doi:10.1172/JCI46229
- MacDonald CJ, Lepage KQ, Eden UT, Eichenbaum H. 2011. Hippocampal “time cells” bridge the gap in memory for discontinuous events. *Neuron* **71**: 737–749. doi:10.1016/j.neuron.2011.07.012
- Maren S. 2001. Neurobiology of Pavlovian fear conditioning. *Annu Rev Neurosci* **24**: 897–931. doi:10.1146/annurev.neuro.24.1.897

- Marks WD, Osanai H, Yamamoto J, Ogawa SK, Kitamura T. 2019. Novel nose poke-based temporal discrimination tasks with concurrent in vivo calcium imaging in freely moving mice. *Mol Brain* **12**: 90. doi:10.1186/s13041-019-0515-7
- Marks WD, Yamamoto N, Kitamura T. 2020. Complementary roles of differential medial entorhinal cortex inputs to the hippocampus for the formation and integration of temporal and contextual memory (Systems Neuroscience). *Eur J Neurosci* doi:10.1111/ejn.14737
- Mattis J, Tye KM, Ferenczi EA, Ramakrishnan C, O'Shea DJ, Prakash R, Gunaydin LA, Hyun M, Fenno LE, Gradinaru V, et al. 2011. Principles for applying optogenetic tools derived from direct comparative analysis of microbial opsins. *Nat Methods* **9**: 159–172. doi:10.1038/nmeth.1808
- McEchron MD, Bouwmeester H, Tseng W, Weiss C, Disterhoft JF. 1999. Hippocampotomy disrupts auditory trace fear conditioning and contextual fear conditioning in the rat. *Hippocampus* **8**: 638–646. doi:10.1002/(SICI)1098-1063(1998)8:6<638::AID-HIPO6>3.0.CO;2-Q
- McEchron MD, Tseng W, Disterhoft JF. 2003. Single neurons in CA1 hippocampus encode trace interval duration during trace heart rate (fear) conditioning in rabbit. *J Neurosci* **23**: 1535–1547. doi:10.1523/JNEUROSCI.23-04-01535.2003
- Misane I, Tovote P, Meyer M, Spiess J, Ogren SO, Stiedl O. 2005. Time-dependent involvement of the dorsal hippocampus in trace fear conditioning in mice. *Hippocampus* **15**: 418–426. doi:10.1002/hipo.20067
- Moore MD, Cushman J, Chandra D, Homanics GE, Olsen RW, Fanselow MS. 2010. Trace and contextual fear conditioning is enhanced in mice lacking the $\alpha 4$ subunit of the GABA_A receptor. *Neurobiol Learn Mem* **93**: 383–387. doi:10.1016/j.nlm.2009.12.004
- Morrissey MD, Maal-Bared G, Brady S, Takehara-Nishiuchi K. 2012. Functional dissociation within the entorhinal cortex for memory retrieval of an association between temporally discontinuous stimuli. *J Neurosci* **32**: 5356–5361. doi:10.1523/JNEUROSCI.5227-11.2012
- Moyer J JR, Deyo RA, Disterhoft JF. 1990. Hippocampotomy disrupts trace eye-blink conditioning in rabbits. *Behav Neurosci* **104**: 243–252. doi:10.1037/0735-7044.104.2.243
- Naya Y, Chen H, Yang C, Suzuki WA. 2017. Contributions of primate prefrontal cortex and medial temporal lobe to temporal-order memory. *Proc Natl Acad Sci* **114**: 13555–13560. doi:10.1073/pnas.1712711114
- Ohara S, Onodera M, Simonsen OW, Yoshino R, Hioki H, Iijima T, Tsutsui KI, Witter MP. 2018. Intrinsic projections of layer Vb neurons to layers Va, III, and II in the lateral and medial entorhinal cortex of the rat. *Cell Rep* **24**: 107–116. doi:10.1016/j.celrep.2018.06.014
- Ohara S, Gianatti M, Itou K, Berndtsson CH, Doan TP, Kitanishi T, Mizuseki K, Iijima T, Tsutsui KI, Witter MP. 2019. Entorhinal layer II calbindin-expressing neurons originate widespread telencephalic and intrinsic projections. *Front Syst Neurosci* **13**: 54. doi:10.3389/fnsys.2019.00054
- Pastalkova E, Itskov V, Amarasingham A, Buzsaki G. 2008. Internally generated cell assembly sequences in the rat hippocampus. *Science* **321**: 1322–1327. doi:10.1126/science.1159775
- Paz R, Pelletier JG, Bauer EP, Pare D. 2006. Emotional enhancement of memory via amygdala-driven facilitation of rhinal interactions. *Nat Neurosci* **9**: 1321–1329. doi:10.1038/nn1771
- Pelkey KA, Chittajallu R, Craig MT, Tricoire L, Wester JC, McBain CJ. 2017. Hippocampal GABAergic inhibitory interneurons. *Physiol Rev* **97**: 1619–1747. doi:10.1152/physrev.00007.2017
- Phillips RG, LeDoux JE. 1992. Differential contribution of amygdala and hippocampus to cued and contextual fear conditioning. *Behav Neurosci* **106**: 274–285. doi:10.1037/0735-7044.106.2.274
- Pilkiw M, Takehara-Nishiuchi K. 2018. Neural representations of time-linked memory. *Neurobiol Learn Mem* **153**: 57–70. doi:10.1016/j.nlm.2018.03.024
- Pilkiw M, Insel N, Cui Y, Finney C, Morrissey MD, Takehara-Nishiuchi K. 2017. Phasic and tonic neuron ensemble codes for stimulus-environment conjunctions in the lateral entorhinal cortex. *eLife* **6**: e28611. doi:10.7554/eLife.28611
- Ray S, Naumann R, Burgalossi A, Tang Q, Schmidt H, Brecht M. 2014. Grid layout and theta-modulation of layer 2 pyramidal neurons in medial entorhinal cortex. *Science* **343**: 891–896. doi:10.1126/science.1243028
- Roth BL. 2016. DREADDs for Neuroscientists. *Neuron* **89**: 683–694. doi:10.1016/j.neuron.2016.01.040
- Runyan JD, Moore AN, Dash PK. 2004. A role for prefrontal cortex in memory storage for trace fear conditioning. *J Neurosci* **24**: 1288–1295. doi:10.1523/JNEUROSCI.4880-03.2004
- Ryou JW, Cho SY, Kim HT. 2001. Lesions of the entorhinal cortex impair acquisition of hippocampal-dependent trace conditioning. *Neurobiol Learn Mem* **75**: 121–127. doi:10.1006/nlme.2000.3966
- Save E, Sargolini F. 2017. Disentangling the role of the MEC and LEC in the processing of spatial and non-spatial information: contribution of lesion studies. *Front Syst Neurosci* **11**: 81. doi:10.3389/fnsys.2017.00081
- Sellami A, Al Abed AS, Brayda-Bruno L, Etchamendy N, Valerio S, Oule M, Pantaleon L, Lamothe V, Potier M, Bernard K, et al. 2017. Temporal binding function of dorsal CA1 is critical for declarative memory formation. *Proc Natl Acad Sci* **114**: 10262–10267. doi:10.1073/pnas.1619657114
- Shu S, Zhu H, Tang N, Chen W, Li X, Li H, Pei L, Liu D, Mu Y, Tian Q, et al. 2016. Selective degeneration of entorhinal-CA1 synapses in Alzheimer's disease via activation of DAPK1. *J Neurosci* **36**: 10843–10852. doi:10.1523/JNEUROSCI.2258-16.2016
- Solomon PR, Vander Schaaf ER, Thompson RF, Weisz DJ. 1986. Hippocampus and trace conditioning of the rabbit's classically conditioned nictitating membrane response. *Behav Neurosci* **100**: 729–744. doi:10.1037/0735-7044.100.5.729
- Stiedl O, Spiess J. 1997. Effect of tone-dependent fear conditioning on heart rate and behavior of C57BL/6N mice. *Behav Neurosci* **111**: 703–711. doi:10.1037/0735-7044.111.4.703
- Suh J, Rivest AJ, Nakashiba T, Tominaga T, Tonegawa S. 2011. Entorhinal cortex layer III input to the hippocampus is crucial for temporal association memory. *Science* **334**: 1415–1420. doi:10.1126/science.1210125
- Surmeli G, Marcu DC, McClure C, Garden DLF, Pastoll H, Nolan MF. 2016. Molecularly defined circuitry reveals input-output segregation in deep layers of the medial entorhinal cortex. *Neuron* **92**: 929. doi:10.1016/j.neuron.2016.11.011
- Suter EE, Weiss C, Disterhoft JF. 2013. Perirhinal and postrhinal, but not lateral entorhinal, cortices are essential for acquisition of trace eyeblink conditioning. *Learn Mem* **20**: 80–84. doi:10.1101/lm.028894.112
- Takehara K, Kawahara S, Kirino Y. 2003. Time-dependent reorganization of the brain components underlying memory retention in trace eyeblink conditioning. *J Neurosci* **23**: 9897–9905. doi:10.1523/JNEUROSCI.23-30-09897.2003
- Takehara-Nishiuchi K, Maal-Bared G, Morrissey MD. 2011. Increased entorhinal-prefrontal theta synchronization parallels decreased entorhinal-hippocampal theta synchronization during learning and consolidation of associative memory. *Front Behav Neurosci* **5**: 90. doi:10.3389/fnbeh.2011.00090
- Tamamaki N, Nojyo Y. 1993. Projection of the entorhinal layer II neurons in the rat as revealed by intracellular pressure-injection of neurobiotin. *Hippocampus* **3**: 471–480. doi:10.1002/hipo.450030408
- Tulving E. 2002a. Chronesthesia: conscious awareness of subjective time. In *Principles of frontal lobe function* (ed. Stuss DT, Knight RT), pp. 311–325. Oxford University Press, Oxford.
- Tulving E. 2002b. Episodic memory: from mind to brain. *Annu Rev Psychol* **53**: 1–25. doi:10.1146/annurev.psych.53.100901.135114
- Varga C, Lee SY, Soltesz I. 2010. Target-selective GABAergic control of entorhinal cortex output. *Nat Neurosci* **13**: 822–824. doi:10.1038/nn.2570
- Volle J, Yu X, Sun H, Nanninen SE, Insel N, Takehara-Nishiuchi K. 2016. Enhancing prefrontal neuron activity enables associative learning of temporally disparate events. *Cell Rep* **15**: 2400–2410. doi:10.1016/j.celrep.2016.05.021
- Wahlstrom KL, Huff ML, Emmons EB, Freeman JH, Narayanan NS, McIntyre CK, LaLumiere RT. 2018. Basolateral amygdala inputs to the medial entorhinal cortex selectively modulate the consolidation of spatial and contextual learning. *J Neurosci* **38**: 2698–2712. doi:10.1523/JNEUROSCI.2848-17.2018
- Wallenstein GV, Eichenbaum H, Hasselmo ME. 1998. The hippocampus as an associator of discontinuous events. *Trends Neurosci* **21**: 317–323. doi:10.1016/S0166-2236(97)01220-4
- Weible AP, McEchron MD, Disterhoft JF. 2000. Cortical involvement in acquisition and extinction of trace eyeblink conditioning. *Behav Neurosci* **114**: 1058–1067. doi:10.1037/0735-7044.114.6.1058
- Wilmot JH, Puhger K, Wiltgen BJ. 2019. Acute disruption of the dorsal hippocampus impairs the encoding and retrieval of trace fear memories. *Front Behav Neurosci* **13**: 116. doi:10.3389/fnbeh.2019.00116
- Woodruff-Pak DS. 2001. Eyeblink classical conditioning differentiates normal aging from Alzheimer's disease. *Integr Physiol Behav Sci* **36**: 87–108. doi:10.1007/BF02734044
- Yang CF, Chiang MC, Gray DC, Prabhakaran M, Alvarado M, Juntti SA, Unger EK, Wells JA, Shah NM. 2013. Sexually dimorphic neurons in the ventromedial hypothalamus govern mating in both sexes and aggression in males. *Cell* **153**: 896–909. doi:10.1016/j.cell.2013.04.017
- Yang X, Yao C, Tian T, Li X, Yan H, Wu J, Li H, Pei L, Liu D, Tian Q, et al. 2018. A novel mechanism of memory loss in Alzheimer's disease mice via the degeneration of entorhinal-CA1 synapses. *Mol Psychiatry* **23**: 199–210. doi:10.1038/mp.2016.151
- Yoshida M, Fransen E, Hasselmo ME. 2008. mGluR-dependent persistent firing in entorhinal cortex layer III neurons. *Eur J Neurosci* **28**: 1116–1126. doi:10.1111/j.1460-9568.2008.06409.x
- Zelikowsky M, Bissiere S, Hast TA, Bennett RZ, Abdipranoto A, Vissel B, Fanselow MS. 2013. Prefrontal microcircuit underlies contextual learning after hippocampal loss. *Proc Natl Acad Sci* **110**: 9938–9943. doi:10.1073/pnas.1301691110

- Zhang L, Chen X, Sindreu C, Lu S, Storm DR, Zweifel LS, Xia Z. 2019. Dynamics of a hippocampal neuronal ensemble encoding trace fear memory revealed by in vivo Ca^{2+} imaging. *PLoS ONE* **14**: e0219152. doi:10.1371/journal.pone.0219152
- Zhou Y, Qiu L, Wang H, Chen X. 2020. Induction of activity synchronization among primed hippocampal neurons out of random dynamics is key for trace memory formation and retrieval. *FASEB J* **34**: 3658–3676. doi:10.1096/fj.201902274R
- Zhu H, Pleil KE, Urban DJ, Moy SS, Kash TL, Roth BL. 2014. Chemogenetic inactivation of ventral hippocampal glutamatergic neurons disrupts consolidation of contextual fear memory. *Neuropsychopharmacology* **39**: 1880–1892. doi:10.1038/npp.2014.35
- Zutshi I, Fu ML, Lilascharoen V, Leutgeb JK, Lim BK, Leutgeb S. 2018. Recurrent circuits within medial entorhinal cortex superficial layers support grid cell firing. *Nat Commun* **9**: 3701. doi:10.1038/s41467-018-06104-5

Received March 15, 2021; accepted in revised form July 8, 2021.